J|A|C|S
ARTICLES
Published on Web 01/11/2002

X-ray Structure Analysis and the Intervalent Electron Transfer in Organic Mixed-Valence Crystals with Bridged Aromatic Cation Radicals

Sergey V. Lindeman, Sergiy V. Rosokha, Duoli Sun, and Jay K. Kochi*

Contribution from the Department of Chemistry, University of Houston, Houston, Texas 77204-5003

Received June 27, 2001. Revised Manuscript Received October 11, 2001

Abstract: X-ray crystallography identifies the aromatic donor group **D** = 2,5-dimethoxy-4-methylphenyl to be a suitable redox center for the construction of organic mixed-valence crystals owing to its large structural change attendant upon 1e oxidation to the cation−radical (**D**$^{\bullet+}$). The combination of cyclic voltammetry, dynamic ESR line broadening, and electronic (NIR) spectroscopy allows the intervalence electron transfer between the redox centers in the mixed-valence system **D**-br-**D**$^{\bullet+}$ [where br can be an aliphatic trimethylene or an aromatic (poly)phenylene bridge] to be probed quantitatively. Independent measures of the electronic coupling matrix element (**H**) for **D**/**D**$^{\bullet+}$ electron exchange via Mulliken−Hush theory accord with the X-ray crystallographic data—both sufficient to consistently identify the various **D**-br-**D**$^{\bullet+}$ according to the Robin−Day classification. Thus, the directly coupled biaryl **D**−**D**$^{\bullet+}$ is a completely *delocalized* cation in class III with the charge distributed equally over both redox centers. The trimethylene- and biphenylene-bridged cations **D**$(CH_2)_3$**D**$^{\bullet+}$ and **D**$(ph)_2$**D**$^{\bullet+}$ with highly *localized* charge distributions are prototypical class II systems involving moderately coupled redox centers with **H** $\approx$ 400 cm^{-1}. The borderline region between class II/III is occupied by the phenylene-bridged cation **D**(ph)**D**$^{\bullet+}$; and the X-ray, CV, and NIR analyses yield ambivalent **H** values (which we believe to be) largely a result of an unusually asymmetric (20/80) charge distribution that is *polarized* between the **D**/**D**$^{\bullet+}$ redox centers.

Introduction

Intramolecular electron transfer between inorganic redox centers (connected by a bridge), originally identified and studied in mixed-valence materials,[1−3] has been increasingly extended to organic redox centers owing to the wide variety of structural possibilities that are potentially available.[4−6] In the latter connection, we now identify the 2,5-dimethoxy-4-methylphenyl group hereinafter designated as **D** to be a particularly useful organic (redox) donor since it undergoes the characteristic quinonoidal distortion upon its 1e oxidation,[7] i.e.

(1) (a) Creutz, C.; Taube, H.*J. Am. Chem. Soc.* **1969**, *91*, 3988; **1973**, *95*, 1086. (b) Creutz, C. *Prog. Inorg. Chem.* **1983**, *30*, 1. (c) Crutchley, R. J. *Adv. Inorg. Chem.* **1994**, *41*, 273. (d) Scandola, F.; Chiorboli, C., Indelli, M. T., Rampi, M. A., Eds. *Electron Transfer in Chemistry*; Wiley-VCH: New York, 2001; Vol. 3.

(2) (a) deSilva, A. P., Ed. Molecular-level Electronics. In *Electron Transfer in Chemistry*; Balzani, V., Ed.; Wiley: New York, 2001; Vol. 5. (b) Tour, J. M. *Acc. Chem. Res.* **2000**, *33*, 791. (c) Roncali, J. *Acc. Chem. Res.* **2000**, *33*, 147. (d) Barigelletti, F.; Flamigni, L. *Chem. Soc. Rev.* **2000**, *29*, 1. (e) Davis, W. B.; Svec, W. A.; Ratner, M. A.; Wasielewski, M. R. *Nature* **1998**, *396*, 60. (f) Bumm, L. A.; Arnold, J. J.; Cygan, M. T.; Dunbar, T. D.; Burgin, T. P.; Jones, L., II; Allara, D. L.; Tour J. M.; Weiss, P. S. *Science* **1996**, *271*, 1705. (g) Lukas, A. S.; Bushard, P. J.; Wasielewski, M. R.; *J. Am. Chem. Soc.* **2001**, *123*, 2440. (h) Fraysse, S.; Coudret, C.; Launay, J.-P. *Eur. J. Inorg. Chem.* **2000**, 1581. (i) Collier, C. P.; Mattersteig, G.; Wong, E. W.; Luo, Y.; Beverly, K.; Sampaio, J.; Raymo, F. M.; Stoddart J. F.; Heath, J. R. *Science* **2000**, *289*, 1172. (j) de Silva, A. P.; Gunaratne, H. Q. N.; Gunnlaugsson, T.; Huxley, A. J. M.; McCoy, C. P.; Rademacher J. T.; Rice, T. E. *Chem. Rev.* **1997**, *97*, 1515.

(3) (a) Jortner, J., Bixon, M., Eds. *Electron Transfer: From Isolated Molecules to Biomolecules, Part 1*; Advances in Chemical Physics; J. Wiley: New York, 1999. (b) Evans, C. E. B.; Naklicki, M. L.; Rezvani, A. R.; White, C. A.; Kondratiev, V. V.; Crutchley, R. J. *J. Am. Chem. Soc.* **1998**, *120*, 13096. (c) For the use of aryl ligands in mixed-valence metal complexes, see: McCusker, J. K.; Jang, H. G.; Wang, S.; Christou, G.; Hendrickson, D. N. *Inorg. Chem.* **1992**, *31*, 1874. (d) Chang, H.-R.; Larsen, S. K.; Boyd, P. D. W.; Pierpont, C. G.; Hendrickson, D. N. *J. Am. Chem. Soc.* **1988**, *110*, 4565. (e) Hendrickson, D. N. Electron Transfer in Mixed-Valence Complexes in Solid State. In *Mixed-Valency Systems: Application in Chemistry, Physics and Biology*; Prassides, K., Ed.; Kluwer Academic Publishers: Hingham, MA, 1991; p 67.

(4) (a) Miller, J. R.; Calcaterra, L. T.; Closs, G. L. *J. Am. Chem. Soc.* **1984**, *106*, 3047. (b) Liang, N.; Miller, J. R.; Closs, G. L. *J. Am. Chem. Soc.* **1989**, *111*, 8740. (c) Liang, N.; Miller, J. R.; Closs, G. L. *J. Am. Chem. Soc.* **1990**, *112*, 5353. (d) Rak, S. F.; Miller, L. L. *J. Am. Chem. Soc.* **1992**, *114*, 1388. (e) Oevering, H.; Paddon-Row: M. N.; Hepperen, M.; Oliver, A. M.; Cotsaris, E.; Verhoeven, J. W.; Hush, N. S. *J. Am. Chem. Soc.* **1987**, *109*, 3258. (f) Penfield, K. W.; Miller, J. R.; Paddon-Row: M. N.; Cotsaris, E.; Oliver, A. M.; Hush, N. S. *J. Am. Chem. Soc.* **1987**, *109*, 5061. (g) Antolovich, M.; Keyte, P. J.; Oliver, A. M.; Paddon-Row: M. N.; Kroon, J.; Verhoeven, J. W.; Jonker S. A.; Warman J. M. *J. Phys.* **1991**, *95*, 1933. (h) Paddon-Row: M. N. *Acc. Chem. Res.* **1994**, *27*, 18.

(5) (a) Nelsen, S. F.; Chang, H.; Wolff, J. J.; Adamus, J. *J. Am. Chem. Soc.* **1993**, *115*, 12276. (b) Nelsen, S. F.; Adamus, J.; Wolff, J. J. *J. Am. Chem. Soc.* **1994**, *116*, 1589. (c) Nelsen, S. F.; Ismagilov, R. F.; Powell, D. R. *J. Am. Chem. Soc.* **1996**, *118*, 6313. (d) Nelsen, S. F.; Ramm, M. T.; Wolff, J. J.; Powell, D. R. *J. Am. Chem. Soc.* **1997**, *119*, 6863. (e) Nelsen, S. F.; Ismagilov, R. F.; Powell, D. R. *J. Am. Chem. Soc.* **1997**, *119*, 10213. (f) Nelsen, S. F.; Tran, H. Q.; Nagy, M. A. *J. Am. Chem. Soc.* **1998**, *120*, 298. (g) Nelsen, S. F.; Ismagilov, R. F.; Powell, D. R. *J. Am. Chem. Soc.* **1998**, *120*, 1924. (h) Nelsen, S. F.; Ismagilov, R. F.; Teki, Y. *J. Am. Chem. Soc.* **1998**, *120*, 2200. (i) Nelsen, S. F.; Ismagilov, R. F.; Gentile, K. E.; Powell, D. R. *J. Am. Chem. Soc.* **1999**, *121*, 7108.

(6) (a) Lahlil, K.; Moradpour, A.; Bowlas, C.; Menou, F.; Cassoux, P.; Bonvoisin, J.; Launay, J.-P.; Dive, G.; Dehareng, D. *J. Am. Chem. Soc.* **1995**, *117*, 9995. (b) Wartini, A. R.; Valenzuela, J.; Staab, H. Z.; Neugebauer, F. A. *Eur. J. Org. Chem.* **1998**, *139*, 9. (c) Lambert, C.; Nöll, G. *J. Am. Chem. Soc.* **1999**, *121*, 8434.

(7) (a) Rathore, R.; Lindeman, S. V.; Kumar A. S.; Kochi, J. K. *J. Am. Chem. Soc.* **1998**, *120*, 6931. (b) Le Maguères, P.; Lindeman, S. V.; Kochi, J. K. *Organometallics* **2001**, *20*, 115.

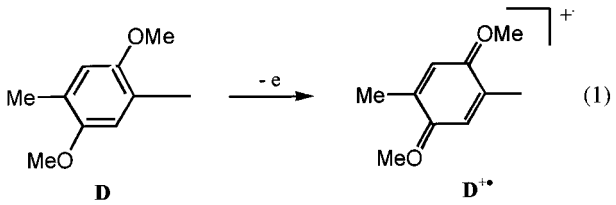

D **D**$^{+\bullet}$ (1)

As such, the use of **D** will allow *partial* electron transfer to be quantitatively evaluated at each redox center of the mixed-valence cation **D**-br-**D**$^{\bullet+}$ (where br denotes the bridge); and a linear regression is sufficient to reliably account for the relatively small (but reproducible) geometric changes in the conjugated (aromatic) π chromophore, i.e.[8]

$$q_i = (d_0 - d_i)/(d_0 - d_1) \qquad (2)$$

where q_i is the partial (positive) charge over a **D** center, d_0 and d_1 are the bond lengths in the neutral **D** and the one-electron oxidized **D**$^{\bullet+}$, respectively, and d_i is the pertinent bond length in a redox-center of the mixed-valence cation.

In this study, we initially exploit X-ray crystallographic analysis to determine the *static* charge distribution in four prototypical mixed-valence systems (MVS)[9] in Chart 1.

The electronic interaction between the redox centers is then revealed in the electrochemical oxidation of the neutral precursor **D**-br-**D**, and the dynamic aspects of intramolecular electron transfer are measured by temperature-dependent ESR line broadening in the cation radical **D**-br-**D**$^{\bullet+}$. Moreover, the characteristic appearance of new intervalence (absorption) bands in the near-IR (spectral) region can be used to test the applicability of the Mulliken−Hush theory for predicting the intramolecular electron-transfer rates in these (organic) mixed-valence systems.

It is especially important to emphasize that the serial use of the experimental techniques of (1) X-ray crystallography, (2) cyclic voltammetry, (3) dynamic ESR line broadening, and (4) electronic (UV−visible) spectroscopy correspond to the increasing time resolution of hours, milliseconds, and nano/picosecond, respectively, that is available for our probing the dynamics of intramolecular electron transfer for the mixed-valence systems included in Chart 1.

Results

I. Structure Analysis of Mixed-Valence Systems by X-ray Crystallography. (A) Structures of D and D$^{\bullet+}$ Centers and the Definition of Charge *q*. The neutral **D** moiety has the usual planar (centrosymmetric) benzenoid geometry, as evaluated from the α−ϵ bond lengths in the structure of the neutral donor **D**(CH$_2$)$_3$**D** (see Table 1 for bond identifications). Thus, the endocyclic α, β, and γ bond lengths are equal to within the standard range of 1.397−1.400 Å.[11] The exocyclic δ and ϵ bond lengths of 1.375(1) and 1.424(1) Å are also very close to the standard values of 1.370 and 1.376 Å, respectively.[11]

Chart 1

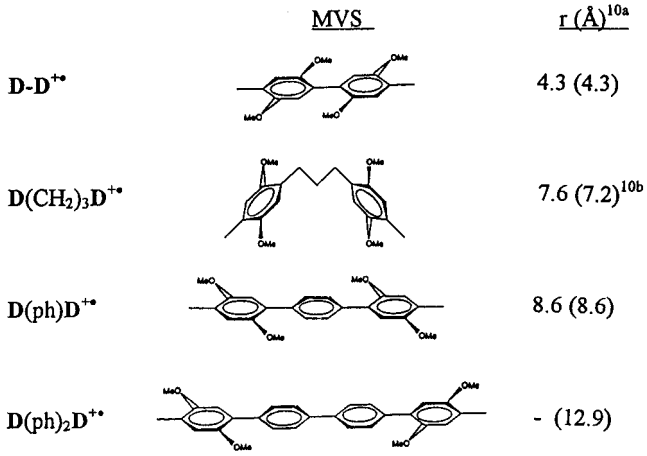

Upon one-electron oxidation, **D** exhibited significant geometric changes as seen from the values of the α−ϵ bond lengths in the dication−diradical **D**$^{\bullet+}$(CH$_2$)$_3$**D**$^{\bullet+}$; (Table 2).[12] This system retains its local center of symmetry, but the α and β bonds become elongated by +4.7 and +1.0 pm, respectively; and the γ bonds are shortened by −2.5 pm in accordance with major resonance contribution of the quinonoid structure (see eq 1). Most remarkably, the exocyclic δ bonds exhibit the greatest change—being shortened by −4.8 pm; and the ϵ bonds are elongated by 3.3 pm. As such, the quinonoid distortion of *p*-dimethoxy-substituted benzenes is a very sensitive geometric measure of their degree of oxidation. In particular, the large magnitude of the geometrical changes allowed us to distinguish (within ±0.1e) among the neutral, cationic, and intermediate (nonintegral) oxidation states of **D** centers.[13] According to definition (eq 2), $q_i = 0$ in **D**(CH$_2$)$_3$**D** and $q_i = +1.0$ for the two equivalent redox centers in **D**$^{\bullet+}$(CH$_2$)$_3$**D**$^{\bullet+}$ (as well as the cationic center in **D**(CH$_2$)$_3$**D**$^{\bullet+}$ [14]).

(B) Charge Distributions in Mixed-Valence Cations. X-ray crystallographic analysis of the cation−radicals of the bridged donors (Chart 1) revealed wide variations in the residual charge q_i on each redox center. For example, the biaryl donor **D**−**D** upon 1e oxidation afforded the dark red crystalline salt **D$_2$**$^{\bullet+}$SbCl$_6^-$ in which both **D** centers are essentially identical.[15] Accordingly, the structure of each redox center in **D**−**D**$^{\bullet+}$ is precisely intermediate between the geometries of the neutral and cationic **D** groups. The values of $q_i = +0.5$ for *each* **D** moiety, as evaluated by the crystallographic data, are listed in Table 2.

The phenylene-bridged cation **D**(ph)**D**$^{\bullet+}$ contains **D** groups that are structurally different from each other—the geometry of

(8) Sun, D.-L.; Lindeman, S. V.; Rathore, R.; Kochi, J. K. *J. Chem. Soc., Perkin Trans. 2* **2001**, 1585.
(9) The synthesis of the neutral precursors **D**-br-**D**, their 1e oxidation to the monocations, and isolation of their crystalline salts for X-ray crystallography are reported separately.[8]
(10) (a) Center-to-center distance *r* in the neutral donor and its cation radical (in parentheses) determined by X-ray crystallography, except as noted otherwise. (b) Taken as the average separation in the neutral donor and dication.
(11) Allen, F. H.; Kennard, O.; Watson, D. G.; Brammer, L.; Orpen A. G.; Taylor, R. *J. Chem. Soc., Perkin Trans. 2* **1987**, S1.
(12) (a) X-ray crystallography establishes the dication of **D**(CH$_2$)$_3$**D** to be the bis(cation radical),[8] the ESR analysis of which will be reported separately. As such, it represents a suitable model for the cationic center in the monocation **D**(CH$_2$)$_3$**D**$^{\bullet+}$ which we have been unable (as yet) to obtain as single crystals for X-ray analysis. (b) The UV−visible and ESR spectra of **D**(CH$_2$)$_3$**D**$^{\bullet+}$ were obtained in solution from the (chemical) comproportionation of the dication (see Experimental Section).
(13) The C−C bond lengths were generally obtained to a precision of $\sigma = 0.003$ Å by low-temperature X-ray crystallography.
(14) In Table 1, (a) the values of q_i were obtained from the δ and ϵ bond lengths. The same results are obtained by using the average change in the bonds. (b) The same values of $q = 0$ and +1.0 were reported earlier.[8] (c) See also footnote 12a.
(15) Importantly, the absence of a crystallographic element of symmetry provided critical evidence for the static nature of the charge distribution in **D**−**D**$^{\bullet+}$ (vide infra).

Table 1. Structural Analysis of the Uncharged (Redox) Center D from the X-ray Crystallography of Various (Bridged) Donors (As Indicated)[a]

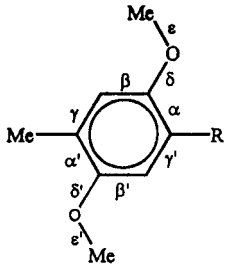

donor	α/α′	β/β′	γ/γ′	δ/δ′	ϵ/ϵ′
DCH_3[b]	1.400	1.397	1.397	1.375	1.424
D$(CH_2)_3$**D**	1.400	1.396	1.397	1.376	1.425
D−**D**[c]	1.401/1.395 [1.398]	1.395/1.400 [1.397]	1.393/1.392 [1.393]	1.373/1.378 [1.375]	1.427/1.426 [1.427]
D(ph)**D**[b]	1.393/1.387 [1.390]	1.395/1.394 [1.395]	1.389/1.402 [1.395]	1.369/1.376 [1.373]	1.425/1.421 [1.423]

[a] All bond distance in Å. Average bond lengths are in brackets. [b] Centrosymmetric. [c] Twofold axis.

Table 2. Geometric Parameters of the Cation Radical Moiety (**D**$^{\bullet+}$) in the Bridged Mixed-Valence Systems (MVS) Included in Chart 1[a]

MVS	[σ][b]	L	α/α′	β/β′	γ/γ′	δ/δ′	ϵ/ϵ′	q_i[c]
[**D**−**D**]$^{\bullet+}$	0.003	**D**^{1}	1.444/1.432 [1.438]	1.400/1.377 [1.389]	1.378/1.408 [1.393]	1.341/1.356 [1.349]	1.453/1.442 [1.447]	+0.5
		D^2	1.442/1.42 [1.433]	1.402/1.383 [1.393]	1.379/1.410 [1.395]	1.344/1.356 [1.350]	1.452/1.442 [1.447]	+0.5
[**D**(ph)**D**]$^{\bullet+}$	0.002	**D**^{1}	1.440/1.436 [1.438]	1.411/1.387 [1.399]	1.377/1.397 [1.387]	1.331/1.344 [1.337]	1.449/1.444 [1.447]	+0.8
		D^2	1.416/1.410 [1.413]	1.399/1.383 [1.391]	1.393/1.409 [1.401]	1.363/1.369 [1.366]	1.432/1.435 [1.433]	+0.2
[**D**$(ph)_2$**D**]$^{\bullet+}$	0.004	**D**^{1}	1.446/1.435 [1.441]	1.411/1.401 [1.406]	1.371/1.383 [1.377]	1.325/1.324 [1.325]	1.454/1.448 [1.451]	+1.0
		D^2	1.410/1.396 [1.403]	1.392/1.392 [1.392]	1.393/1.410 [1.401]	1.370/1.385 [1.377]	1.440/1.419 [1.429]	0.0
D$^{\bullet+}(CH_2)_3$**D**$^{\bullet+}$	0.004	**D**^{1}	1.447/1.447 [1.447]	1.407/1.408 [1.407]	1.369/1.375 [1.372]	1.324/1.329 [1.327]	1.457/1.457 [1.457]	+1.0
		D^2	1.447/1.447 [1.447]	1.407/1.408 [1.407]	1.369/1.375 [1.372]	1.324/1.329 [1.327]	1.457/1.457 [1.457]	+1.0

[a] Average bond lengths (Å) in brackets. [b] Average experimental precision (Å). [c] Positive charge parameter evaluated according to eq 2.

one **D** being closer to the neutral **D**, whereas the other **D** has a more cationic geometry. Both **D**s differed significantly from either a pure neutral or cationic **D** center, and quantitative evaluation according to eq 2 yielded an asymmetric charge distribution of $q_i = 0.2$ and $q_i = 0.8$.

The biphenylene-bridged cation **D**$(ph)_2$**D**$^{\bullet+}$ contained the most unsymmetrical charge distribution since the geometry of one **D** center did not exhibit any geometric changes relative to that extant in the neutral donor **D**$(ph)_2$**D**, whereas the other reproduced the standard geometry of a cationic **D** group (see Table 2). In other words, it followed from eq 2 that the completely unsymmetrical distribution of charge was $q_i = 0$ and $q_i = +1.0$ at each end of the mixed-valence cation.

(C) Conformational Changes Attendant upon 1e Oxidation of D-br-D Donors to the Mixed-Valence Cations. Substantial changes in molecular shapes, particularly those involving conformations about the D−br bond, accompanied their 1e oxidation. Thus, the neutral **D**−**D** with essentially orthogonal redox centers exhibits substantial planarization upon its conversion to the mixed-valence cation. In particular, the twist of $\varphi = 69.1°$ about the C−C bond in **D**−**D** was decreased to $\varphi = 39.5°$ in **D**−**D**$^{\bullet+}$ (Figure 1), and this was accompanied by a concomitant bond *shortening* from 1.491 to 1.458 Å.

Compared to **D**−**D**$^{\bullet+}$, the sterically less hindered phenylene-bridged cation **D**(ph)**D**$^{\bullet+}$ is (expectedly) less twisted around the pair of symmetrically equivalent **D**−br bonds by $\varphi = 44.9°$. Upon oxidation, the twist is even more reduced to $\varphi = 32.1°$ and 28.6°—with the simultaneous shortening of the **D**−br bond from 1.493 to 1.466 and 1.474 Å. Remarkably, the shorter **D**−br bond is associated with that **D** having the more pronounced cationic geometry.

The conformational structure of the biphenylene-bridged cation **D**$(ph)_2$**D**$^{\bullet+}$ is similar to that of **D**(ph)**D**$^{\bullet+}$ (Figure 2), the dihedral angles being $\varphi = 36.7°$ and 31.7° (the twist between the phenylene rings is 17.0°). The intercyclic (ph−ph) bond *increases* regularly (from 1.469 to 1.485 and to 1.488 Å) on proceeding from the positively charged to the neutral donor.

It is particularly noteworthy that a consistent set of geometrical parameters is applicable to **D** groups in **D**$(CH_2)_3$**D** as well as those with phenylene and biphenylene bridges. Even the direct connection of the redox centers (as in the directly coupled **D**−**D** donor) does not significantly perturb these geometric parameters. To evaluate the electronic interaction between a pair of bridged **D** groups, we initially noted that the property of **D** is such that it shows no significant intermolecular association upon oxidation, i.e., **D** + **D**$^{\bullet+} \neq$ (**D**$_2$)$^{\bullet+}$, as opposed to many other aromatic electron donors (naphthalene, anthracene, etc.).[16] Consequently, intramolecular effects can be readily differentiated from those derived from self-associations. Accordingly, we now turn to transient electrochemical methods to evaluate the interaction between redox centers upon 1e oxidation of the **D**-br-**D** donors to the mixed-valence cations.

II. Formation Energetics of Mixed-Valence Cations by Transient Electrochemical Methods. (A) Cyclic Voltammetric Behavior of D as an Electron Donor. The mononuclear donor **D**−CH_3 readily underwent a reversible 1e electrochemical oxidation in dichloromethane solution (containing 0.1 M tetrabutylammonium hexachloroantimonate) at $E^\circ_{ox} = 1.10$ V versus SCE.[17] Similarly, the binuclear donor **D**$(CH_2)_3$**D** also showed a chemically reversible cyclic voltammetric wave at $E^\circ_{ox} = 1.10$ V (Figure 3), but coulometric calibration established the anodic oxidation to be a 2e process—to indicate that

(16) Le Maguères, P.; Lindeman, S. V.; Kochi, J. K. *J. Chem. Soc., Perkin Trans. 2* **2001**, 1180.

(17) The cation radical **D**$CH_3^{\bullet+}$ of the mononuclear donor (electrochemically generated at $E_{ox} = 1.10$ V) was readily reduced back to the neutral donor quantitatively.

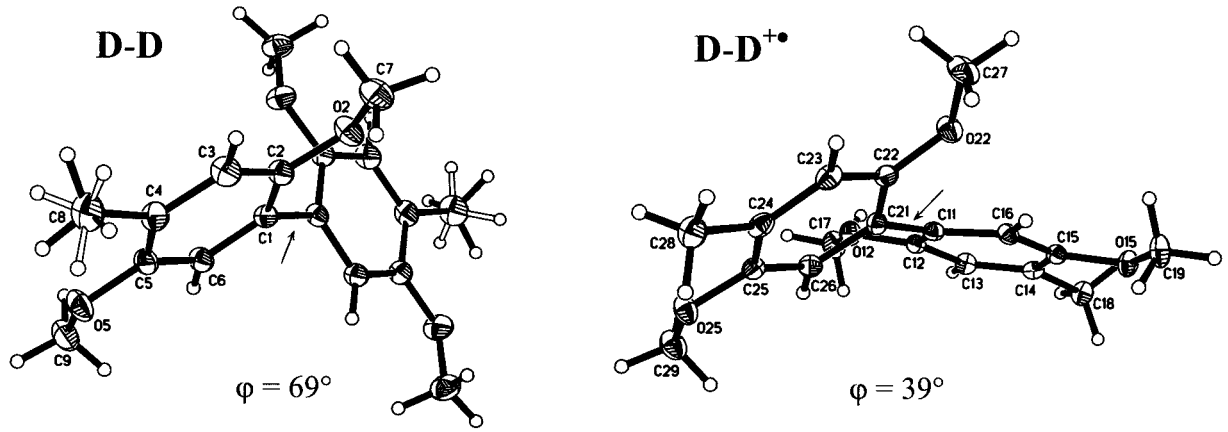

Figure 1. ORTEP diagrams of (left) the biaryl donor (**D**−**D**) and (right) its cation radical (as the hexachloroantimonate salt) with the arrows pointing to the relevant aryl−aryl bond (i.e., C1−C1′ and C21−C11, respectively). Note the cisoid conformation of **D**−**D** and the transoid conformation of **D**−**D**$^{\bullet+}$ upon one-electron oxidation.

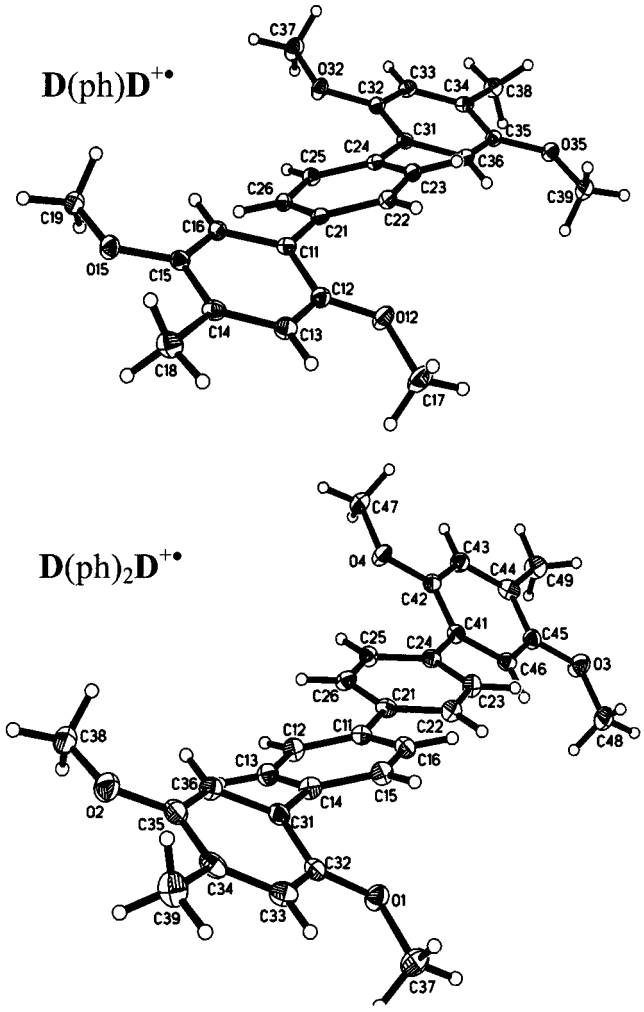

Figure 2. Conformations of (upper) the phenylene-bridged cation radical **D**(ph)**D**$^{\bullet+}$ and (lower) the biphenylene-bridged cation radical **D**(ph)$_2$**D**$^{\bullet+}$ showing their overall (near-planar) structures).

both **D** groups were oxidized more or less independently. Thus, the latter supported the X-ray crystallographic results (vide infra) that the redox centers in **D**$(CH_2)_3$**D**$^{\bullet+}$ effected no (or minimal) electronic perturbations on each other.

(B) Electronic Interaction of Redox Centers in Mixed-Valence Cations. The cyclic voltammetry of the directly coupled biaryl **D**−**D** showed two distinctly resolved and chemically reversible waves at $E^{\circ}_{ox} = 1.11$ and 1.40 V versus SCE. Since coulometry established that both CV waves consisted of 1e oxidations, we concluded that the production of the cation radical **D**−**D**$^{\bullet+}$ was separately followed by its oxidation to the dication **D**−**D**$^{2+}$. The potential difference of $\Delta E_{ox} = 0.29$ V thus quantitatively indicated that the oxidation of the second **D** was negatively affected by presence of the first **D**$^{+}$ center. This observation was again consistent with the X-ray results showing the significant electronic perturbation between the redox centers in **D**−**D**$^{\bullet+}$. Such an effect on the energetics is inherent to the comproportionation (equilibrium) constant K_{com} of this mixed-valence cation, i.e.

$$\mathbf{D}-\mathbf{D}^{2+} + \mathbf{D}-\mathbf{D} \overset{K_{com}}{\rightleftharpoons} 2\mathbf{D}-\mathbf{D}^{\bullet+} \qquad (3)$$

and the free-energy change for the reversible equilibrium in eq 3 can be evaluated as $\Delta G_{com} = -RT \ln K_{com}$, where $\Delta G_{com} = -\mathcal{F}\Delta E_{ox}$.

The cyclic voltammetric behavior of the phenylene-bridged mixed-valence cation **D**(ph)**D**$^{\bullet+}$ was somewhat similar, in that the first and second CV waves were resolved (see Figure 3), but the splitting of $\Delta E_{ox} = 0.11$ V (see Table 3) was significantly less than that of the directly coupled cation **D**−**D**$^{\bullet+}$. However, the further extension of the bridge to biphenylene resulted in a different cyclic voltammetry behavior, and **D**(ph)$_2$**D** showed only a single 2e wave that was quite reminiscent of that in **D**$(CH_2)_3$**D** (compare Figure 3c and d).

The distinctive cyclic voltammetry behavior of these mixed-valence cations suggested a profound modulation of the electronic perturbation between the redox centers by the connecting bridge. To examine this difference further, we turned to the magnetic resonance properties of the paramagnetic mixed-valence cations.

III. Intramolecular Electron-Transfer Rates from Temperature-Dependent ESR Spectra of Mixed-Valence Cations. (A) ESR Spectrum of the Prototypical Redox Center (D$^{\bullet+}$). Electrochemical or chemical oxidation[18] of the mononuclear donor **D**CH_3 served for the prototypical generation of the redox center (**D**$^{\bullet+}$) in mixed-valence cations at 0 °C in dichloromethane solution. The ESR spectrum of **D**$CH_3^{\bullet+}$ was characterized by

(18) Rathore, R.; Kumar, A. S.; Lindeman S. V.; Kochi, J. K. *J. Org. Chem.* **1998**, *63*, 5847.

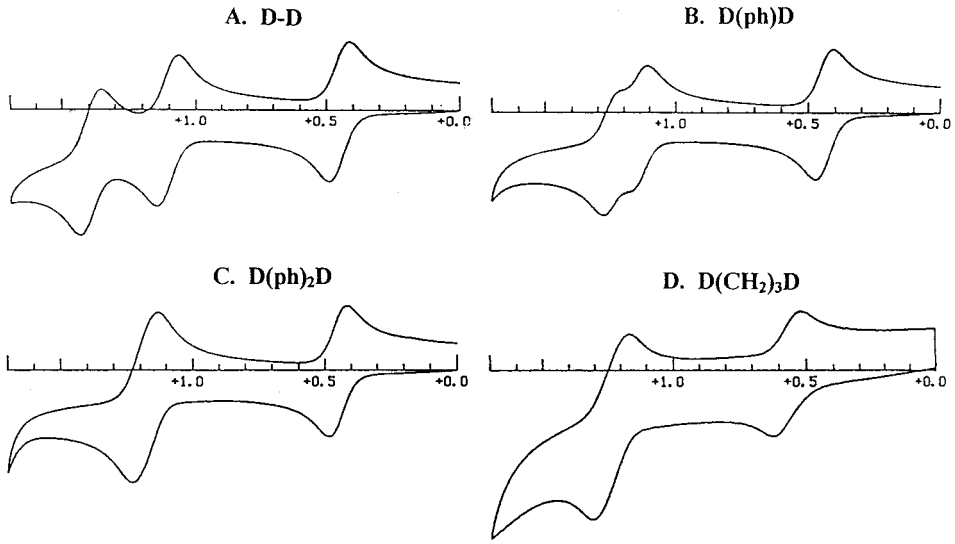

Figure 3. Cyclic voltammograms (initial positive scan) of the bridged mixed-valence systems in Chart 1 measured in dichloromethane containing 0.1 M tetrabutylammonium hexafluorophosphate at a scan rate of 2 V s^{-1}. The calibration of each cyclic voltammograms is represented by the first reversible wave, which corresponds to that of the ferrocene internal standard.

Table 3. Cyclic Voltammetry of Bridged Aromatic Donors[a]

donor	E_{ox1}[b](1)	E_{ox2}[b](2)	ΔE_{ox}
D−**D**	1.11 (1e)	1.40 (1e)	0.29
D(ph)**D**	1.15 (1e)	1.26 (1e)	0.11
D$(ph)_2$**D**	1.18 (2e)		
D$(CH_2)_3$**D**	1.10 (2e)		
DCH_3	1.10 (1e)		

[a] Oxidation potentials given in V (±0.03) vs SCE. [b] Number of electron transferred in parentheses.

three sets of proton splitting: $a_{OMe} = 3.12$ G (6H), $a_{Me} = 4.37$ G (6H), and $a_{CH} = 0.48$ G (2H).[19] Similar hyperfine splittings pertained to the cation radical **D**(ph)$H^{\bullet+}$ (See Figure 1S in Supporting Information), which is the closest mononuclear analogue of the phenylene-bridged mixed-valence cations. The ESR spectra of **D**$CH_3^{\bullet+}$ and **D**(ph)$H^{\bullet+}$ were singularly invariant (within the experimental observation) when the solutions were gradually cooled to −100 °C.

(B) Temperature-Dependent (ESR) Line Broadening in Mixed-Valence Cations. The ESR spectrum of the biphenylene-bridged mixed-valence cation **D**$(ph)_2$**D**$^{\bullet+}$ at −120 °C was essentially identical with that of the mononuclear analogue **D**(ph)$H^{\bullet+}$ (vide supra). However, as the temperature was gradually raised to 18 °C, Figure 4 (left) shows the progressive line broadening of the ESR spectrum, which we attributed to the dynamic electron exchange between the pair of redox centers in **D**$(Ph)_2$**D**$^{\bullet+}$. Computer simulation of this intramolecular process was carried out with the aid of the ESR-EXN program;[20] and Figure 4 (right) shows the fit to the experimental ESR spectrum with typical first-order rate constants of $k_{exc} = 1 \times 10^7$ s^{-1} at −105 °C and $k_{exc} = 3 \times 10^9$ s^{-1} at 18 °C.

The ESR spectrum of the trimethylene-bridged cation **D**$(CH_2)_3$**D**$^{\bullet+}$ was difficult to measure at low temperature owing to experimental difficulties.[21] Nevertheless, the partially resolved ESR spectrum obtained at −80 °C could be simulated with the aid of the hyperfine splittings obtained for the model (mononuclear) cation radical **D**(Ph)$H^{\bullet+}$ if additional hyperfine splittings for the trimethylene bridge were included (see Figure 2S in Supporting Information). On raising the temperature to 20 °C, the spectrum broadened to a single (unresolved) absorption (Figure 2S, left) reminiscent of that for **D**$(ph)_2$**D**$^{\bullet+}$. Our inability to precisely simulate the partially resolved ESR spectrum (merely) allowed us to estimate the first-order rate processes as $k_{exc} > 10^8$ s^{-1} at 20 °C and $k_{exc} \leq 10^7$ s^{-1} at −90 °C.

(C) Temperature-Independent (ESR) Line Broadening in Mixed-Valence Cations. The ESR spectrum of the directly coupled biaryl cation radical **D**−**D**$^{\bullet+}$ showed no temperature-dependent change between 22 and −90 °C. The experimental ESR spectrum illustrated in Figure 5A (left) was satisfactorily simulated in Figure 5A (right) using proton hyperfine coupling constants with (a) half the magnitude and including (b) twice the number of nuclei as those in the reference cation **D**$CH_3^{\bullet+}$. Such a behavior indicated a delocalized (electronic) system with the charge distributed equally on each redox center.[8]

The temperature-dependent behavior of the phenylene-bridged cation **D**(ph)**D**$^{\bullet+}$ was intermediate between the static **D**−**D**$^{\bullet+}$ and the dynamic **D**$(ph)_2$**D**$^{\bullet+}$ and tending more toward the former. Thus, the more-or-less same (well-resolved) ESR spectrum in Figure 5B (left) was observed in the temperature range between 20 and −100 °C, and the computer-simulated spectrum in Figure 5B (right) was obtained with hyperfine splitting constants similar to those for **D**−**D**$^{\bullet+}$. However, a careful scrutiny of the ESR line widths showed slightly larger line widths for **D**(ph)**D**$^{\bullet+}$ relative to **D**−**D**$^{\bullet+}$. As such, this study indicated that the charge distributions in both cations are essentially indistinguishable on the ESR time scale.

IV. Intervalence (Absorption) Bands in the Electronic Spectra of Mixed-Valence Cations. (A) UV−Visible Absorption Spectrum of D and D$^{\bullet+}$ Chromophores. The electronic spectrum of the mononuclear prototype **D**CH_3 was characterized by a pair of intense UV absorptions [$\lambda_{max} = 201$ nm ($\epsilon_{201} = 3 \times 10^4$ M^{-1} cm^{-1}) and $\lambda_{max} = 290$ nm ($\epsilon_{290} = 4 \times 10^3$ M^{-1} cm^{-1})] and by the absence of further low-energy bands in the

(19) Forbes, W. F.; Sullivan, P. D. *J. Phys. Chem.* **1968**, *48*, 1411.
(20) Heinzer, J. *Quantum Chemistry Program Exchange* 209, as modified by P. A. Petillo and R. F. Ismagilov. We thank Prof. S. F. Nelsen for a copy of this program.
(21) Since we were unable to grow single crystals of the **D**$(CH_2)_3$**D**$^{\bullet+}$ salt, the ESR spectrum in Figure 2S was obtained via the comproportionation of **D**$(CH_2)_3$**D**$^{2+}$ with large amount of neutral donor.[12]

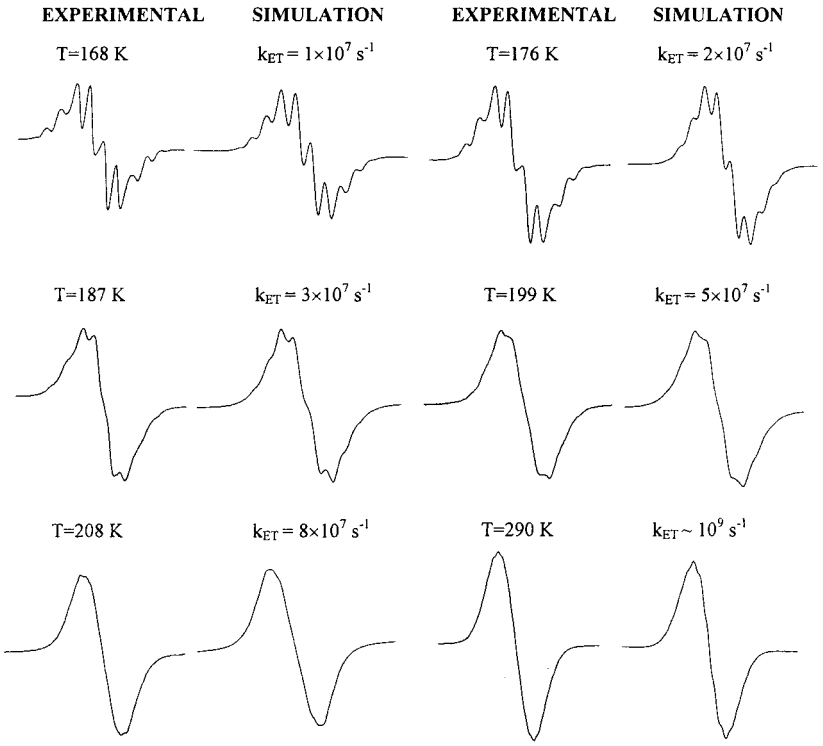

Figure 4. Temperature-dependent ESR (X-band) line broadening of the biphenylene-bridged cation radical $\mathbf{D}(ph)_2\mathbf{D}^{\bullet+}$ (left side) in comparison with computer-simulated spectra (right side) for first-order (electron) exchange.

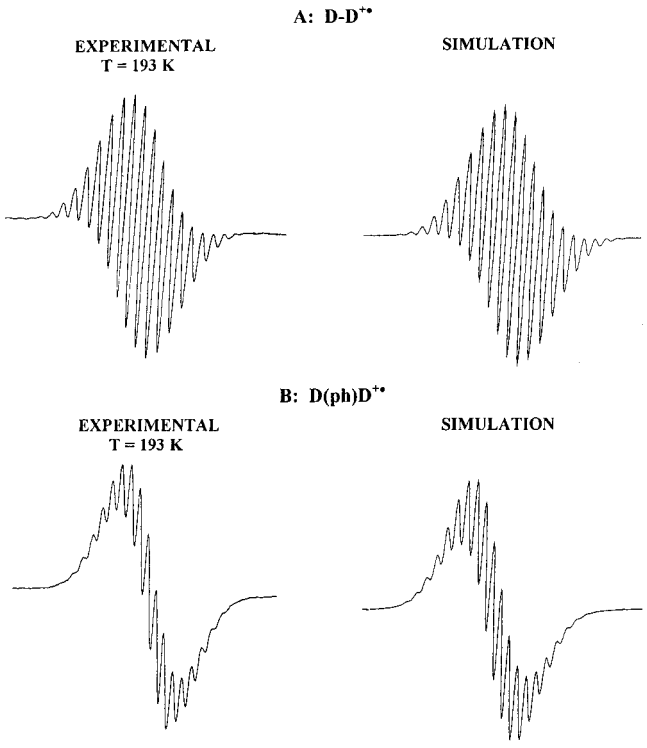

Figure 5. Comparison of the ESR spectra of (A) the coupled biaryl cation radical $\mathbf{D}-\mathbf{D}^{\bullet+}$ and (B) the phenylene-bridged cation radical $\mathbf{D}(ph)\mathbf{D}^{\bullet+}$ with the computer-simulated spectra on the right.

visible−NIR spectral region. Oxidation to $\mathbf{D}CH_3^{\bullet+}$ resulted in the appearance of a rather intense band at $\lambda_{max} = 462$ nm ($\epsilon_{462} = 1 \times 10^4\ M^{-1}\ cm^{-1}$) with a shoulder at 448 nm and an additional weak band at $\lambda_{max} = 650$ nm.

(B) Electronic Spectrum of the Trimethylene-Bridged Cation $\mathbf{D}(CH_2)_3\mathbf{D}^{\bullet+}$. The electronic spectrum of $\mathbf{D}(CH_2)_3\mathbf{D}^{\bullet+}$ in the UV−visible region was similar to that of $\mathbf{D}CH_3^{\bullet+}$, but it differed significantly in the NIR region by the appearance of an intense absorption $\lambda_{max} = 1500$ nm ($\epsilon_{1500} = 1.2 \times 10^4\ M^{-1}\ cm^{-1}$) shown in Figure 6. This NIR band disappeared upon the oxidation of $\mathbf{D}(CH_2)_3\mathbf{D}^{\bullet+}$ to its dication (vide supra). Since the relative intensities of the 460- and 1500-nm bands were independent of the concentration of $\mathbf{D}(CH_2)_3\mathbf{D}^{\bullet+}$, the NIR band was clearly connected with an intramolecular (electronic) transition of the intervalence type described in Table 4.

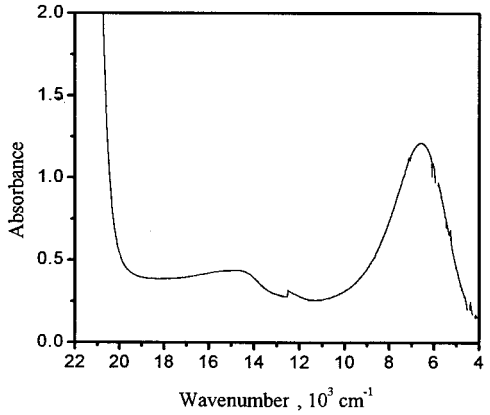

Figure 6. Electronic spectrum of the trimethylene-bridged cation radical $\mathbf{D}(CH_2)_3\mathbf{D}^{\bullet+}$ in the low-energy region showing the prominent intervalence (absorption) band at $\nu_{max} = 6.70 \times 10^3\ cm^{-1}$.

(C) Intervalence Bands in the Phenylene-Bridged Cations $\mathbf{D}(ph)\mathbf{D}^{\bullet+}$ and $\mathbf{D}(ph)_2\mathbf{D}^{\bullet+}$. The electronic spectrum of $\mathbf{D}(ph)\mathbf{D}^{\bullet+}$ showed a strong NIR absorption at 6400 cm^{-1} (Figure 7), which disappeared upon its further oxidation to the dication. Moreover, this intervalence (NIR) band was absent in the mononuclear prototype $\mathbf{D}(ph)H^{\bullet+}$. The digital deconvolution of the low-energy band revealed its (pure) Gaussian band shape (see Figure 7, right). Figure 7 also shows the presence of new

Table 4. Comparative Electronic Spectra of Bridged Cation Radicals (CR = **D**-br-**D**$^{\bullet+}$), Their Dications (DC = **D**-br-**D**$^{2+}$), and the Mononuclear (Model) Cation−Radical (MC = **D**-br-H$^{\bullet+}$)[a]

system	CR$^{(\bullet+)}$		DC$^{(2+)}$		MC$^{(\bullet+)}$	
D−**D**		2150 (4.8)				
D$(CH_2)_3$**D**		1500 (1.2)				
D(ph)**D**	620 (2.2)	1570 (3.9)	550 (2.6)	910 (1.6)	540 (7.4)	910 (2.0)
D$(ph)_2$**D**	660 (2.3)	1330 (4.5)	640 (6.1)	1130 (5.5)	640 (2.7)	1140 (3.0)

[a] In dichloromethane solution at 20 °C. Absorption in nm and extinction coefficient. (parentheses) in 10^3 M^{-1} cm^{-1}.

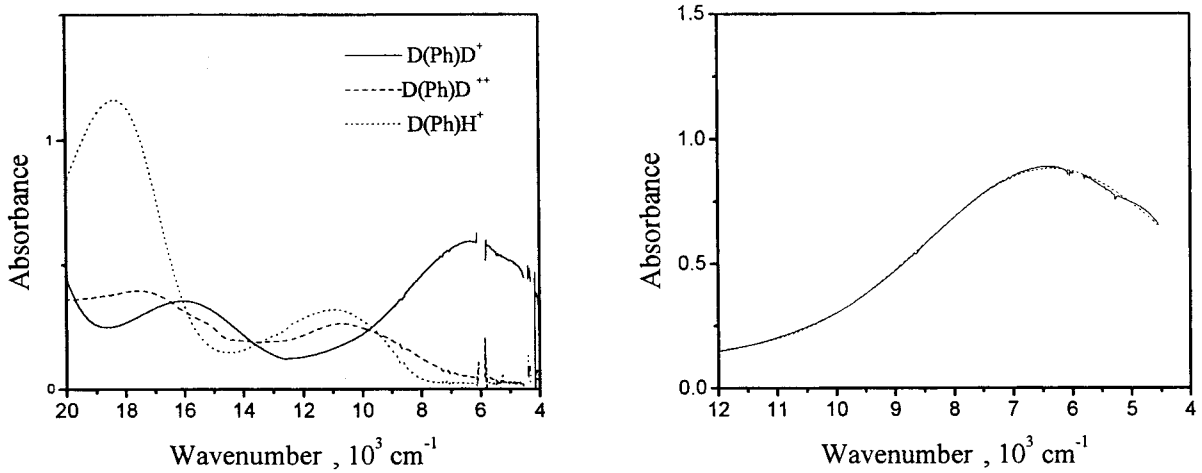

Figure 7. (Left) Spectral comparison of the phenylene-bridged cation radical **D**(ph)**D**$^{\bullet+}$ with its dication[8] **D**$^{\bullet+}$(ph)**D**$^{\bullet+}$ and the mononuclear model cation radical **D**(ph)H$^{\bullet+}$. (Right) Digital subtraction of the lowest-energy band of **D**$^{\bullet+}$(ph)**D**$^{\bullet+}$ from that of **D**(ph)**D**$^{\bullet+}$ to reveal the spectral difference as the (Gaussian) intervalence band with $\nu_{max} = 6.37 \times 10^3$ cm^{-1}.

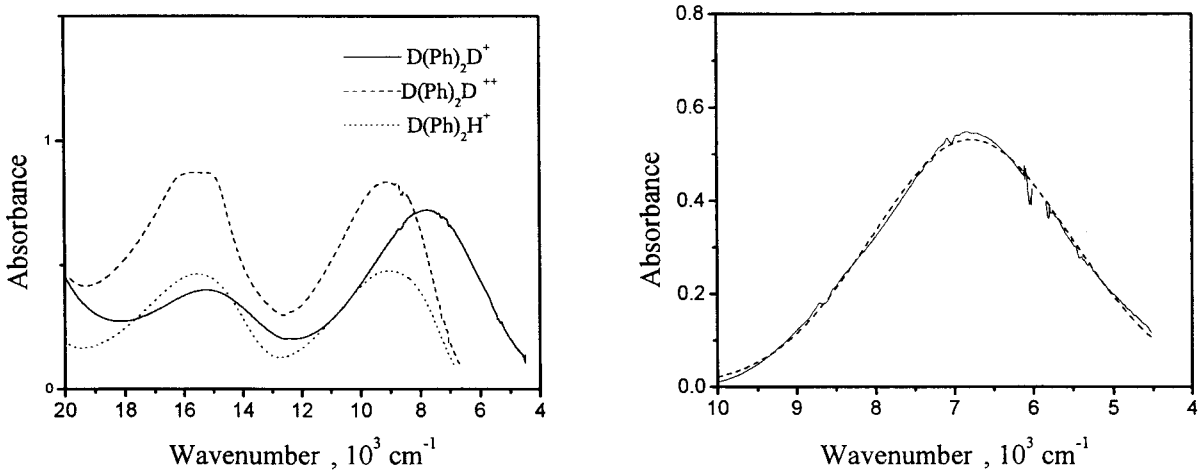

Figure 8. (Left) Electronic spectrum of the mixed-valence system **D**$(ph)_2$**D**$^{\bullet+}$ showing the prominent (composite) NIR band relative to the bridge-to-redox center (b → D$^{\bullet+}$) absorptions in **D**$^{\bullet+}(ph)_2$**D**$^{\bullet+}$ and **D**$(ph)_2$H$^{\bullet+}$. (Right) Gaussian deconvolution to reveal the intervalence (NIR) band of the biphenylene-bridged cation−radical **D**$(ph)_2$**D**$^{\bullet+}$ as in Figure 5.

UV−visible band that was also present in the dication **D**(ph)-**D**$^{2+}$ as well as in the mononuclear prototype **D**(ph)H$^{\bullet+}$—but singularly absent in either alkyl analogue **D**$CH_3^{\bullet+}$ or **D**$(CH_2)_3$**D**$^{\bullet+}$. Thus, these UV−visible bands were readily identified with the intramolecular interaction of **D**$^{\bullet+}$ with the aromatic (ph) bridge (otherwise denoted as metal/ligand or ligand/metal transition in metal-centered redox systems[22]).

The electronic spectrum of the biphenylene-bridged cation **D**$(ph)_2$**D**$^{\bullet+}$ (Figure 8) was quite similar to that of the lower homologue **D**(ph)**D**$^{\bullet+}$—with the exception that only the NIR band was shifted from 6400 to 7500 cm^{-1}. Oxidation to the dication **D**$(ph)_2$**D**$^{2+}$ resulted in the further blue shift to 8800 cm^{-1}. It is noteworthy that the electronic spectrum of the dication **D**$(ph)_2$**D**$^{2+}$ and the mononuclear prototype **D**$(ph)_2$H$^{\bullet+}$ were virtually superimposable.

(D) Electronic Spectrum of the Static Biaryl Cation−Radical D−D$^{\bullet+}$. The low-energy (NIR) absorption band of **D**−**D**$^{\bullet+}$ was strongly red-shifted to $\lambda_{max} = 2150$ nm, but otherwise, the UV−visible band at $\lambda_{max} = 580$ nm was only slightly blue-shifted from that of the phenylene- and the biphenylene-bridged analogues. The digital deconvolution of the NIR spectral envelope in Figure 9 revealed three Gaussian

(22) This band assignment is consistent with its being observed only with the phenylene- and biphenylene-bridged cations but not with the (aliphatic) trimethylene-bridged analogue. Further, the red-shift of biphenylene (relative to the phenylene) system is expected from its better electron donor ability.

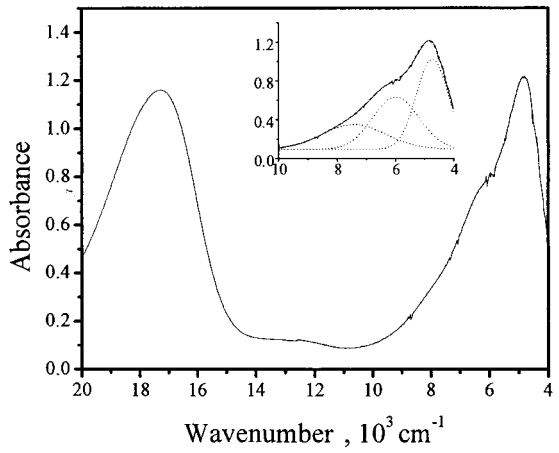

Figure 9. Electronic spectrum of the coupled biaryl cation radical **D**−**D**$^{\bullet+}$ in the low-energy region showing the clearly separated NIR (absorption) band. (Inset) Gaussian deconvolution of the NIR envelope to reveal the intervalence band with $\nu_{max} = 4.66 \times 10^3$ cm^{-1}.

components (Figure 9, right), with the lowest energy band being the most intense.

Discussion

The organic donor **D** (identified in eq 1) serves as an excellent redox center for the construction of new mixed-valence systems that are cast in the classical (inorganic) mold. [1−3] As such, we believe that the Robin−Day classification[23] can be used to identify three basic structural types of these mixed-valence cations.

I. X-ray Crystallographic Identification of the Class III/Class II Interface. The basic distinction between class III and class II systems according to Robin and Day is the ground-state structure of mixed-valence systems—class III relating to the single potential well as opposed to the two-state model often invoked with class II systems. In our organic systems, the precise X-ray crystallography achieved at low temperature can alone offer an unambiguous method for the definitive investigation of ground-state structures as follows.

(A) The Biaryl Cation−Radical D−D$^{\bullet+}$ as a Robin−Day Class III System. We have shown in Tables 1 and 2 that the biaryl cation radical **D**−**D**$^{\bullet+}$, with 50% charge on each redox center, is a static system residing in a single potential energy well. However, the observed changes in molecular geometry and derived values of q_i can be questioned in several ways. For example, such a result can arise from a fast *oscillation* between chemically equivalent charge-localized forms within the crystal, i.e.

$$\mathbf{D}-\mathbf{D}^{+} \rightleftarrows \mathbf{D}^{+}-\mathbf{D} \qquad (4)$$

Alternatively, this might obtain from static crystalline disorder resulting in a statistical distribution of randomly polarized (right- and left-handed) localized forms that are "frozen" over the entire crystal. If either of these scenarios were to pertain,[24] the observed geometry of **D** moieties must *perforce* be an exact linear combination of the neutral and cationic **D** forms—in other words, the value of q_i in eq 2 must be the same for all (bond-length) parameters (α−ϵ; see Tables 1 and 2) in any given structure.[16] This is clearly not so—the most significant deviation of the observed geometry of **D** moieties in **D**−**D**$^{\bullet+}$ from a simple linear combination of pure **D** and pure **D**$^{\bullet+}$ being the loss of a local symmetry center.[15] In other words, the geometric parameters α and α′, β and β' are no longer equivalent in these moieties, and in particular, the values of δ are always shorter than δ'.[25] The latter is especially indicative that the (distonic) charge redistribution between the redox centers in **D**−**D**$^{\bullet+}$ involves the central (inter-ring) bond—which suffers significant shortening (vide supra). The latter in valence bond terminology can be the result of π conjugation arising from the resonance contribution of the *acentric o*-quinonoid structure **Q**′ to the charge delocalization, in addition to the usual *centrosymmetric p*-quinonoid contribution **Q** (see eq 1 and Scheme 1), where the generic br represents the redox center **D** in the biaryl mixed-valence system. On the basis of Paulings' bond-length/bond-order relationship,[26] we estimate that there is as much as 30% π conjugation between the redox centers in **D**−**D**$^{\bullet+}$.[8]

Scheme 1

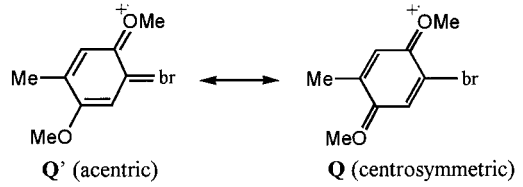

(B) The Biphenylene-Bridged Cation D(ph)2D$^{\bullet+}$ as a Robin−Day Class II System. X-ray structural analysis points to **D**(ph)$_2$**D**$^{\bullet+}$ as a classical Robin−Day class II system since each redox center retains the primary structure of **D** and **D**$^{\bullet+}$ intact within an estimated precision of ∼5%. The same conclusion applies to the trimethylene-bridged cation **D**(CH$_2$)$_3$**D**$^{\bullet+}$. In both cases, the cyclic voltammetric analysis of the donor oxidation in Table 3, as well as the low-temperature ESR spectra of the mixed-valence cations, supports the same conclusion.

(C) The Phenylene-Bridge Cation D(ph)D$^{\bullet+}$ as a Borderline Class II/III System. Structurally, the phenylene-bridged **D**(ph)**D**$^{\bullet+}$ is the most distinctive mixed-valence cation, due to the presence of **D** moieties which reflect neither the neutral nor the monocationic redox centers. The asymmetric charge distribution of 20/80 established by X-ray analysis (vide supra) represents the *static* electron population of the ground-state cation for the same crystallographic reasons presented above for the 50/50 charge distribution in **D**−**D**$^{\bullet+}$. In other words, the biphenylene-bridged cation represents a *polarized* structure with the "center" of the π electron density shifted closer to one end than to the other. Again, such a polarization can be attributed to π conjugation between the redox center **D**$^{\bullet+}$ and the phenylene bridge, and from the bond contraction described above, we estimate the degree of π conjugation between the central phenylene bridge (br) to each of the terminal redox centers to be ∼20% and 10%.[27] As such, we prefer to describe the electronic structure of **D**(ph)**D**$^{\bullet+}$ as *"polarized"* since it is

(23) Robin, M. B.; Day, P. *Adv. Inorg. Chem. Radiochem*. **1967**, *10*, 247.
(24) The X-ray crystallographic literature is rife with such examples. See, e.g.: Darovsky, A.; Kezerashvili, V.; Coppens, P.; Weyhermüller, T.; Hummel, H.; Wieghardt, K. *Inorg. Chem*. **1996**, *35*, 6916.
(25) Such an inequality points to a large acentric *o*-quinonoid resonance contribution **Q**′ in addition to the centrosymmetric *p*-quinonoid structure **Q**.
(26) Pauling, L. *Nature of the Chemical Bond*; Cornell: Ithaca, NY, 1960; p 280.
(27) By comparison, in the biphenylene-bridged cation, the π conjugation does not spread out from 15% with the first phenylene group and is barely detectable beyond that.

Chart 2

MVS	X_{min}	R-D Class
$\mathbf{D}(CH_2)_3\mathbf{D}^{+\bullet}$	0	II
$\mathbf{D}(ph)_2\mathbf{D}^{+\bullet}$	0	II
$\mathbf{D}(ph)\mathbf{D}^{+\bullet}$	0.2	II/III
$\mathbf{D}\text{-}\mathbf{D}^{+\bullet}$	0.5	III

intermediate between the completely delocalized $\mathbf{D}-\mathbf{D}^{\bullet+}$ and the undelocalized (static) $\mathbf{D}(ph)_2\mathbf{D}^{\bullet+}$ and $\mathbf{D}(CH_2)_3\mathbf{D}^{\bullet+}$ structures.

For intramolecular electron transfer, the ground-state wave function for the two-state model contains contributions from the initial and final states.[28] We summarize in Chart 2 the positions of the reactant minimum (X_{min}) along the reaction coordinate for the various mixed-valence systems based on the X-ray results.

Thus, $\mathbf{D}(CH_2)_3\mathbf{D}^{\bullet+}$ and $\mathbf{D}(ph)_2\mathbf{D}^{\bullet+}$ both with $X_{min} = 0$ represent Robin−Day class II systems that are characterized by a pair of weakly interacting states. The biaryl cation $\mathbf{D}-\mathbf{D}^{\bullet+}$ with $X_{min} = 0.5$ (and confirmed by its ESR spectrum in Figure 5A), belongs in class III. The phenylene-bridged cation $\mathbf{D}(ph)\text{-}\mathbf{D}^{\bullet+}$ with a similar ESR behavior (Figure 5B) also seems to fall in class III. However, the CV coupling of $\Delta E_{ox} = 0.11$ V, which is only somewhat greater than those in $\mathbf{D}(CH_2)_3\mathbf{D}^{\bullet+}$ and $\mathbf{D}(ph)_2\mathbf{D}^{\bullet+}$, as well as the slight shift of the reactant minimum to $X_{min} = 0$, provides some ambivalence toward class II. Taken all together, the X-ray, CV, and ESR probes point to the phenylene-bridged cation $\mathbf{D}(ph)\mathbf{D}^{\bullet+}$ as a class II system in which the sizable electronic coupling between the redox centers $\mathbf{D}/\mathbf{D}^{\bullet+}$ leads to (strongly) adiabatic electron transfer.

To provide a more quantitative description of the intramolecular electron transfer, we now turn to the intervalence absorption bands observed in the NIR spectral region (Figures 6−9) of all the mixed-valence cations in Chart 1.

II. Electronic Coupling of $\mathbf{D}/\mathbf{D}^{\bullet+}$ Centers in Mixed-Valence Cations. In the framework of the semiclassical model for electron transfer,[29] the electronic coupling matrix element **H** is basic to the evaluation of the electronic factors governing the pairwise interaction of redox centers in the mixed-valence cation.[30] Using the Mulliken formalism,[31] Hush showed that the electronic coupling matrix element in class II systems is[32]

$$\mathbf{H} = 0.0206(\nu_{max}\Delta\nu_{1/2}\epsilon)^{1/2}/r \qquad (5)$$

where ν_{max} and $\Delta\nu_{1/2}$ are the maximum and full width at half-heights, respectively (in cm^{-1}), of the intervalence absorption band, ϵ is the molar extinction coefficient at the absorption maximum (in M^{-1} cm^{-1}), and r is the distance between redox centers (in Å). Moreover, in class II systems, the energy of the intervalence band is directly related to the Marcus reorganization energy λ of the $\mathbf{D}/\mathbf{D}^{\bullet+}$ redox centers, i.e., $\nu_{max} = \lambda$.[29,30]

(A) The Trimethylene and Biphenylene-Bridged Mixed-Valence Cations as Prototypical Class II Systems. In $\mathbf{D}(CH_2)_3\mathbf{D}^{\bullet+}$, the intervalence band is clearly resolved as a single Gaussian band at $\lambda_{max} = 1500$ nm shown in Figure 8. As a class II system, the electronic coupling element is $\mathbf{H} = 400$ cm^{-1} based on eq 5 with $\nu_{max} = 6.7 \times 10^3$ cm^{-1} (Table 4), $\Delta\nu_{1/2} = 2.4 \times 10^3$ cm^{-1}, $\epsilon = 1.2 \times 10^3$ M^{-1} cm^{-1}, and $r = 7.2$ Å (Chart 1). By comparison, the resonance stabilization of the mixed-valence cation, i.e. [30]

$$\Delta G_r = -2\mathbf{H}^2/\lambda \qquad (6)$$

is only $\Delta G_r = 48$ cm^{-1}, which is indeed too small to be resolved (in accord with our CV experiments in Table 3).[33]

Application of the same theoretical (spectral) treatment to the biphenylene-bridged cation $\mathbf{D}(ph)_2\mathbf{D}^{\bullet+}$ is predicated upon the deconvolution of the NIR spectral envelope to afford the (resolved) intervalence band with $\nu_{max} = 6.8 \times 10^3$ cm^{-1} shown in Figure 8B.[34] The electron coupling element of $\mathbf{H} = 430$ cm^{-1} is strikingly similar to that of the trimethylene analogue when $\nu_{max} = 6.8 \times 10^3$ cm^{-1} (Table 4), $\Delta\nu_{1/2} = 2.5 \times 10^3$ cm^{-1}, $\epsilon = 4.2 \times 10^3$ M^{-1} cm^{-1}m and $r = 12.9$ Å (Chart 1) calculated according to eq 5. The resonance stabilization calculated on the basis of eq 6 is 54 cm^{-1}, which again is too small to be resolved in the CV experiments.[33] Moreover, the calculated shift of the reactant minimum based on eq 7,[30] is too small (0.002) to be

$$X_{min} = {}^1/_2[1 - (1 - 4\mathbf{H}^2/\lambda^2)^{1/2}] \qquad (7)$$

resolved in our X-ray measurements (where no shifts of the charge from the neutral to the cationic redox center are observed).

(B) The Biaryl Cation $\mathbf{D}-\mathbf{D}^{\bullet+}$ as a Class III System. The electronic spectrum of the biaryl cation $\mathbf{D}-\mathbf{D}^{\bullet+}$ consists of two primary bands—a Gaussian VIS band at $\lambda_{max} = 580$ nm and a complex NIR envelope, which could be deconvoluted into three Gaussian components (Figure 9B). We attribute the low-energy (NIR) absorption to strong mutual $\mathbf{D}/\mathbf{D}^{\bullet+}$ interaction, as also revealed by the X-ray, CV, and ESR results (vide supra). On the basis of the PMO theory,[35] we assign the most intense low-energy band with $\lambda_{max} = 2150$ nm to the electronic transition from the bonding to antibonding orbital of the strongly interacting pair of redox (HOMO/SOMO) centers, i.e. Chart 3.

The presence of the pair of additional (higher energy) Gaussian components in the composite NIR absorption of $\mathbf{D}-\mathbf{D}^{\bullet+}$ in Figure 9 is assigned to the resolved vibrational structure of the bonding-to-antibonding electronic transition. [In other words, the most intense (lowest energy) component corresponds to the 0,0 band, and the other two bands, with energy about 6100 and 7500 cm^{-1} are assigned to the 0,1 and 0,2 transitions.[36]] In either case, the electronic coupling matrix element for $\mathbf{D}-\mathbf{D}^{\bullet+}$ can be evaluated directly from $\lambda_{max} = 2150$ nm, since $\mathbf{H} = \nu_{max}/2$ for class III systems.[30] The value of $\mathbf{H} =$

(28) Creutz, C.; Newton, M. D.; Sutin, N. *J. Photochem. Photobiol. A: Chem.* **1994**, *82*, 47.
(29) (a) Marcus, R. A. *J. Chem. Phys.* **1957**, *26*, 867. (b) Marcus, R. A. *Discuss. Faraday Soc.* **1960**, *29*, 21. (c) Marcus, R. A. *J. Phys. Chem.* **1963**, *67*, 853. (d) Marcus, R. A. *J. Chem. Phys.* **1965**, *43*, 679.
(30) Sutin, N. *Prog. Inorg. Chem.* **1983**, *30*, 441. See also: Sutin, N. *Adv. Chem. Phys.* **1999**, *106*, 7. Brunschwig, B. S.; Sutin, N. *Coord. Chem. Rev.* **1999**, *187*, 233.
(31) Mulliken, R. S.; Person, W. B. *Molecular Complexes*; Wiley: New York, 1969.
(32) (a) Hush, N. S. *Prog. Inorg. Chem.* **1967**, *8*, 391. (b) Hush, N. S. *Electrochim. Acta* **1968**, *13*, 1005. (c) Hush, N. S. *Coord. Chem. Rev.* **1984**, *60*, 107.
(33) Note that the difference in (CV) redox potentials ΔE_{ox} in bridged donors (Table 3) is directly related to the comproportionation constant in eq 3, i.e., $\Delta E_{ox} = \Delta G_{com}/F$, where F is the Faraday constant. Although ΔG_{com} includes nonresonance terms (e.g., solvation, electronic interaction, etc,), they are generally minor relative to the electronic interaction ΔG_r.
(34) For the deconvolution of the NIR envelope, see Figure 9 (inset). The lowest-energy Gaussian component is assigned to the intervalence transition and the residual high-energy components to the (**D**-br) charge-transfer transitions.[22]
(35) Dewar, M. J. S.; Dougherty, R. C. *The PMO Theory of Organic Chemistry*; Plenum Press: New York, 1975.

Chart 3

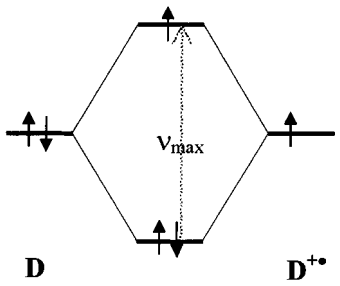

2330 cm^{-1} (0.29 eV), which is substantially larger than those for either $\mathbf{D}(CH_2)_3\mathbf{D}^{\bullet+}$ or $\mathbf{D}(ph)_2\mathbf{D}^{\bullet+}$, reflects the strong electronic interaction extant in the biaryl cation.[36b] The latter can also be viewed from the perspective of the comproportionation equilibrium (in eq 3) based on the CV data. Since the free-energy change ΔG_{com} is a strong reflection of the resonance stabilization ΔG_r for large values of ΔE_{ox} (Table 3),[33] it follows from the class III relationship[30]

$$\Delta G_r = -2(\mathbf{H} - \lambda/4) \qquad (8)$$

that the reorganization energy for the closely coupled $\mathbf{D}-\mathbf{D}^{\bullet+}$ is $\lambda = 0.58$ eV. Such a value of the reorganization energy supports the classification of $\mathbf{D}-\mathbf{D}^{\bullet+}$ as a Robin−Day class III system.[23]

(C) The Phenylene-Bridged Cation at the Class II/III Border. In the phenylene-bridged cation $\mathbf{D}(ph)\mathbf{D}^{\bullet+}$, the NIR band in Figure 7B is red-shifted (relative to the biphenylene analogue in Figure 8B) and approaches that of the directly coupled biaryl cation $\mathbf{D}-\mathbf{D}^{\bullet+}$ in Figure 9B. If $\mathbf{D}(ph)\mathbf{D}^{\bullet+}$ is taken as a class II system, then the value of the reorganization energy λ is 0.79 eV since $\lambda = \nu_{max}$.[29,30] The calculated value of electronic coupling element is $\mathbf{H} = 770$ cm^{-1} (0.095 eV) based on eq 5 and $\nu_{max} = 6.4 \times 10^3$ cm^{-1}, $\Delta\nu_{1/2} = 4.1 \times 10^3$ cm^{-1}, $\epsilon = 3900$ M^{-1} cm^{-1}, and $r = 8.6$ Å. However, the electronic coupling element can also be evaluated from the difference of the redox potentials $\Delta E_{ox} = \Delta G_r/F$ (when contributions from nonresonance stabilizations are neglected).[33] With the aid of eq 5 and $\lambda = 0.79$ eV, **H** is alternatively calculated to be 0.21 eV, which is more than twice that obtained for a class II system according to eq 5. Furthermore, the value of the electronic coupling element estimated from the X-ray result (which yields $X_{min} = 0.2$ in Chart 2) and eq 7 is $\mathbf{H} = 0.31$ eV. Accordingly, let us next examine the correspondence of **H** with the electron-transfer dynamics in the hope of resolving such discrepancies.

III. Intramolecular Electron Transfer in the Mixed-Valence Cation. The dynamics of intramolecular electron transfer in the biaryl cation $\mathbf{D}-\mathbf{D}^{\bullet+}$ as a class III system relate to the completely delocalized cation radical with the activation free energy $\Delta G^{\ddagger} = 0$. Indeed, we confirm such a delocalization in the invariant ESR spectra at all (accessible) temperatures. The intramolecular electron transfer in class II mixed-valence cations (of interest here) is theoretically evaluated from the electronic spectra which provide direct access to the activation free energy, i.e.[30]

$$\Delta G^{\ddagger} = (\lambda - 2\mathbf{H})^2/4\lambda \qquad (9)$$

where λ is the Marcus reorganization energy of the redox centers and **H** is the resonance integral to represent the $\mathbf{D}/\mathbf{D}^{\bullet+}$ electronic interaction energy in the class II mixed-valence cation.[30] Thus, the evaluation of λ and **H** from the NIR spectra provides the kinetics basis for intramolecular electron transfer.

Table 5. Mulliken−Hush Calculation of the Electronic Coupling Elements from the Intervalence (Absorption) Band

MVS	r, Å	ν_{IV}, 10^3 cm^{-1}	$\Delta\nu_{IV}$,[a] 10^3 cm^{-1}	**H**, cm^{-1}	$\Delta G^{\ddagger}$, kcal/mol
$\mathbf{D}-\mathbf{D}^{\bullet+}$	4.3	4.66	*b*	2330[c]	0
$\mathbf{D}(ph)\mathbf{D}^{\bullet+}$	8.6	6.37	4.1	760[d]	2.6
$\mathbf{D}(ph)_2\mathbf{D}^{\bullet+}$	12.9	6.79	2.5	430[d]	3.7
$\mathbf{D}(CH_2)_3\mathbf{D}^{\bullet+}$	7.2	6.70	2.4	400[d]	3.7

[a] Band full width at half-height. [b] Low-energy absorption consists of three Gaussian bands. [c] Taken as $\nu_{max}/2$. [d] From Mulliken−Hush eq 5.

The activation free energies for intramolecular electron transfer in the trimethylene- and biphenylene-bridged cations (calculated from eq 9, together with **H** and λ values listed in Table 5), are both $\Delta G^{\ddagger} = 3.7$ kcal M^{-1}. A comparable value of the activation free energy $\Delta G^{\ddagger} = 4.2$ kcal M^{-1} is obtained (see Figure 3S in Supporting Information) from the temperature-dependent rate constants obtained from the ESR line-broadening experiments for $\mathbf{D}(ph)_2\mathbf{D}^{\bullet+}$ in Figure 4. Thus, the similar line-broadening behavior of $\mathbf{D}(CH_2)_3\mathbf{D}^{\bullet+}$ in Figure 2S is consistent with the theoretical values of $\Delta G^{\ddagger}$ in Table 5. As such, the intramolecular dynamics of the electron-transfer processes evaluated experimentally by dynamic ESR studies are in reasonable agreement with the theoretical evaluations based on moderate values of the electronic coupling element and the reorganization energies associated with $\mathbf{D}/\mathbf{D}^{\bullet+}$ interchange in these class II cations.

In the phenylene-bridged cation, the ESR line-broadening behavior (Figure 5B) suggests a low barrier for intramolecular electron transfer, as characterized for a delocalized cation radical. However, the electron-transfer rates calculated from the optical, X-ray, and CV data, as summarized in Table 6, are highly variable. Although the absence of a reliable value of preexponential factor[37] does not allow us to come to a definitive conclusion, the value of the $\exp(-\Delta G^{\ddagger}/RT)$ term obtained from the optical data appears to be too small (see columns 5 and 6), especially at low temperature.[38] Such ET rates would have resulted in a substantially greater temperature dependence as well as significantly greater line broadening of the ESR spectrum shown in Figure 5. Indeed, the values of **H** based on the CV and X-ray results appear to be more in line with the experimental ESR data. A number of reasons are possible for the discordant

(36) (a) Similar composite NIR bands in class III systems were observed previously[5,6a] and assigned to resolved vibrational structure.[5f] Alternatively, the higher energy bands may be due to electronic transition from subjacent HOMO of the bridged cation radical $\mathbf{D}-\mathbf{D}^{\bullet+}$. (b) Optical transitions in class III systems do not involve charge transfer and are not accompanied by a net dipole moment change.[30] Nonetheless, the Mulliken−Hush formulation can (in principle) be employed within a two-state model for the calculation of **H** in class III systems[28,30]—but does leave open the questions as to the proper choice of r and the band assignments. If we arbitrarily take $r = 4.3$ Å, the calculated values of **H** is 640 cm^{-1} (0.08 eV), based on eq 9, and $\nu_{max} = 4650$ cm^{-1}, $\Delta\nu_{1/2} = 1100$ cm^{-1}, and $\epsilon = 3500$. However, if all the NIR bands are summed, the calculated $\mathbf{H} = 1950$ cm^{-1} (0.24 eV) is in reasonable (considering the uncertainty in r) agreement with the values calculated from $H = \nu_{max}/2$ for class III systems (vide infra).

(37) (a) Theoretical methods are available for the calculation of the preexponential factor from the charge-transfer band shape[32c] and the values of **H**.[30] Since we are unable to make reliable calculations in our system, the arbitrary preexponential factor of 10^{12} was uniformly taken. (b) See also: Elliot, C. M.; Derr, D. L.; Matyushov, D. V.; Newton, M. D. *J. Am. Chem. Soc.* **1998**, *120*, 11714.

(38) For example, the ESR spectra of other bridged systems with $\exp(-\Delta G^{\ddagger}/RT) \cong 10^{-4}$ and $k_{ET} \sim 10^8$ lead to broadened (unresolved) ESR spectra (unpublished results).

Table 6. Intramolecular Electron Exchange Parameters for the Phenylene-Bridged Cation−Radical **D**(ph)**D**$^{\bullet+}$. Comparison with the Mulliken−Hush Theory

method	**H**,[a] cm^{-1}	$\Delta G^{\ddagger}$,[b] kcal/mol	$\exp(-\Delta G^{\ddagger}/RT)$[c] 20 °C	$\exp(-\Delta G^{\ddagger}/RT)$[c] 100 °C	k_{ET}[c] 20 °C	k_{ET}[c] 100 °C
Mulliken−Hush	770	2.6	0.012	3×10^{-4}	10^{10}	3×10^{8}
cyclic voltammetry	1600	1.0	0.17	0.04	2×10^{11}	4×10^{10}
X-ray crystallography	2400	0.2	0.7	0.5	7×10^{11}	5×10^{11}

[a] See Discussion, section IIC. [b] From eq 9. [c] For $k_{ET} = 10^{12} \exp(-\Delta G^{\ddagger}/RT)$.

kinetics results for **D**(ph)**D**$^{\bullet+}$. First, the Mulliken−Hush eq 9 may require an adjustment for mixed-valence systems on (or close to) the class III/II border. Second, the simple distance term (r) in eq 9 may also lose significance in the borderline region.[39] Third, rather minor errors in the experimental parameters (such as in the charge q_i from the X-ray results) can have a large effect on **H** according to eq 3. Fourth, the relationship of the equilibrium free-energy change with the CV difference in the redox change ΔE_{ox} may require a more rigorous consideration. Such an ambiguity in the treatment of **D**(ph)**D**$^{\bullet+}$ is reminiscent of the long-standing difficulty in the class II/III assignment of the Creutz−Taube (ruthenium-based) mixed-valence system that afforded similar contradictory results from different experimental techniques.[16] Nonetheless, the general trend in the **D/D**$^{\bullet+}$-based system is clear—with the electronic interaction term decreasing in the following order: **D**−**D**$^{\bullet+}$ > **D**(ph)**D**$^{\bullet+}$ > **D**$(ph)_2$**D**$^{\bullet+}$ ≈ **D**$(CH_2)_3$**D**$^{\bullet+}$, which is more dependent on the nature of the bridge than the distances that separate the **D/D**$^{\bullet+}$ centers (compare Chart 1). As such, we will address this point in the following part of this study.[40]

Summary and Conclusions

X-ray crystallography is employed for the first time to successfully delineate the (electronic) charge distribution between a pair of aromatic (redox) centers in mixed-valence systems, in an unbridled effort to extend the classic (inorganic) prototypes[l] by including their (versatile) organic counterparts. Thus, the static (positive) charge q_i on each aromatic center (**D**) in the mixed-valence cation **D**-br-**D**$^{\bullet+}$ is found to be the following: (a) $q_i = 0$ and 1.0 in **D**$(ph)_2$**D**$^{\bullet+}$ (where br = *p*-biphenylene), (b) $q_i = 0.5$ and 0.5 in the directly coupled biaryl cation **D**-**D**$^{\bullet+}$, and (c) $q_i = 0.2$ and 0.8 in the phenylene-bridged cation radical **D**-(ph)-**D**$^{\bullet+}$—as Robin−Day examples of class II, class III, and borderline class II/III systems, respectively. Cyclic voltammetric behavior of the donors **D**-br-**D** as well as dynamic ESR line broadening of the cation radicals **D**-br-**D**$^{\bullet+}$ provides ample support for the X-ray-based classification. Most importantly, the theoretical analysis of the diagnostic NIR (absorption) bands extant in the electronic spectra of all the mixed-valence cations (Chart 1) lead to the quantitative evaluation of the electronic coupling matrix element **H** between the **D/D**$^{\bullet+}$ centers by the application of Mulliken−Hush theory of intervalence electron exchange.[32] Calculations of the activation free energy ($\Delta G^{\ddagger}_{ET}$) lead to first-order rate constants (k_{ET}) that are in agreement with the experimental electron-transfer rates (based on ESR line broadening) and verify the Robin−Day classification that stems from the X-ray structural analysis (and CV and ESR measurements).

(39) Especially in view of the asymmetric (20/80) charge distribution in **D**(ph)**D**$^{\bullet+}$.
(40) Rosokha, S. V.; Sun, D.-H.; Kochi, J. K., manuscript to be submitted.

Experimental Section

Materials. Dichloromethane and toluene were purified according to published procedures.[41] 2,5-Dimethoxytoluene,[7] 2,5-dimethyl-1,4-dimethoxybenzene,[7] 4,4′-dimethyl-2,5,2′,5′-tetramethoxy-1,1′-biphenyl (**D**−**D**),[8] bis(2,5-dimethoxy-4-methylphenyl)propane[8] (**D**$(CH_2)_3$**D**), 4,4″-dimethyl-2,5,2″,5″-tetramethoxy-1,1′:4′,1″-terphenyl (**D**(ph)**D**),[8] and 4,4‴-dimethyl-2,5,2‴,5‴-tetramethoxy-1,1′:4′,1″:4″,1‴-quaterphenyl (**D**$(ph)_2$**D**)[8] were prepared according to the literature procedure, as well as the precursor of 2,3,8,9-tetrahydro-1,1,4,4,7,7,10,10-octamethyltetracene radical−cation (**OMN**$^{\bullet+}$).[7] All of the compounds were characterized by melting points, IR, ^{1}H NMR, ^{13}C NMR, MS, and elemental analysis.

Instrumentation. The ^{1}H NMR spectra were recorded in $CDCl_3$ on a General Electric QE-300 NMR spectrometer. Infrared spectra were recorded on a Nicolet 10 DX FT spectrometer. Gas chromatography was performed on a Hewlett-Packard 5890A gas chromatograph equipped with a HP 3392 integrator. GC−MS analyses were carried out on a Hewlett-Packard 5890 gas chromatograph interfaced to a HP 5970 mass spectrometer.

X-ray crystallographic analysis was carried out with aid of a Siemens SMART diffractometer equipped with a CCD detector using Mo Kα radiation ($\lambda = 0.710\ 73$ Å) typically at −150 °C. The structures were solved by direct methods[42] and refined by a full matrix least-squares procedure with IBM Pentium and SGI O_2 computers.[43] The X-ray crystallographic parameters and the details of the refinements for the neutral donors and their cation radicals salts are presented in Table 7 (See also Supporting Information).

Cyclic Voltammetry. Cyclic voltammetry (CV) was performed on a BAS 100A electrochemical analyzer with a cell of airtight design with high-vacuum Teflon valves and Viton O-ring seals to allow an inert atmosphere to be maintained without contamination by grease. The working electrode consisted of an adjustable platinum disk embedded in a glass seal to allow periodic polishing (with a fine emery cloth) without significant changing the surface area (∼1 mm^2). The saturated calomel electrode (SCE) and its salt bridge were separated from the cathode by a sintered glass frit. The counter electrode consisted of a platinum gauze that was separated from the working electrode by ∼3 mm. The measurements were carried out in a solution of 0.1 M supporting electrolyte (tetra-*n*-butylammonium hexafluorophosphate) and 5×10^{-4} M compound in dry dichloromethane under an argon atmosphere. All cyclic voltammograms were measured at a uniform sweep rate of 2 V s^{-1} (with *iR* compensation). The potentials were referenced to SCE, which was calibrated with added ferrocene (5×10^{-4} M). Controlled-potential coulometry was conducted with an EG&G Princeton Applied Research (PAR) 173 potentiostat and digital coulometer. The number of electrons transferred was calculated from the relation $n = Q/Fm$, where F is the Faraday constant, m is the moles of the material, and Q is the number of coulombs passed at the time the current dropped to <3−9% of its original value.

(41) Perrin, D. D.; Armagero, W. L.; Perrin, D. R. *Purification of Laboratory Chemicals*, 2nd ed.; Pergamon: New York, 1980.
(42) Sheldrick, G. M. *SHELXS-86*, Program for Structure Solution; University of Göttingen: Göttingen, Germany, 1986.
(43) There is a rotational disorder of a terminal methyl group in the structure of the neutral donor **D**−**D** (see Figure 1). There is also rotational disorder of the central *p*-phenylene ring in the structure of the neutral donor **D**(ph)**D**.

Table 7. Crystallographic Data for Aromatic Donors and Their Cation Radicals

	DCH_3	**D**$(CH_2)_3$**D**	**D**$^+(CH_2)_3$**D**$^+$	**D**–**D**	**D**–**D**$^+$	**D**(ph)**D**	**D**(ph)**D**$^+$	**D**$(ph)_2$**D**$^+$
empirical formula	$C_{10}H_{14}O_2$	$C_{21}H_{28}O_4$	$C_{21}H_{28}O_4^{2+}2SbCl_6^-$	$C_{18}H_{22}O_4$	$C_{18}H_{22}O_4^+SbCl_6^-$	$C_{24}H_{26}O_4$	$C_{24}H_{26}O_4^+SbCl_6^-$	$C_{30}H_{30}O_4^+SbCl_6^-$
formula wt	166.21	344.43	1013.33	302.36	636.81	378.45	712.90	788.99
cryst syst	monoclinic	orthorhombic	monoclinic	monoclinic	triclinic	triclinic	monoclinic	monoclinic
space group	$P2_1/n$	$P2_12_12_1$	$P2_1/m$	$C2/c$	P-1	P-1	$P2_1/c$	$P2_1$
a, Å	6.4943(4)	7.8130(5)	8.073(2)	22.199(11)	7.6596(2)	5.0760(3)	13.4765(2)	7.2182(1)
b, Å	8.9209(5)	7.9994(5)	26.577(5)	5.8270(3)	12.8575(3)	13.962(1)	15.5512(3)	16.6646(3)
c, Å	8.0240(5)	29.763(2)	8.445(2)	12.6965(7)	13.7700(3)	14.341(1)	13.8393(3)	13.4314(1)
α, deg	90	90	90	90	62.369(1)	77.796(2)	90	90
β, deg	101.82(1)	90	98.99(3)	109.85	83.190(1)	88.587(2)	105.94(1)	103.88(1)
γ, deg	90	90	90	90	83.567(1)	88.641(2)	90	90
V, Å^3	455.02(5)	1860.2(2)	1789.6(6)	1544.8(1)	1190.5(1)	992.9(1)	2788.8(1)	1568.44(4)
Z	2	4	2	4	2	2	4	2
T, K	123(2)	93(2)	123(2)	123(2)	123(2)	123(2)	123(2)	123(2)
μ, mm^{-1}	0.083	0.084	2.432	0.091	1.855	0.085	1.594	1.426
ρ_{calc}, g/cm^3	1.213	1.230	1.881	1.300	1.777	1.266	1.698	1.671
total refl	4073	23294	22003	10207	17125	10726	34861	23274
unique refl	1987	4699	8082	3439	10303	5993	12599	13253
data [$I > 2\sigma(I)$]	1593	4102	5945	1847	7229	2535	9054	9677
params	57	338	190	103	271	295	322	376
R_1[a]	0.049	0.039	0.047	0.058	0.045	0.099	0.037	0.046
wR_2[b]	0.120	0.094	0.093	0.137	0.070	0.233	0.071	0.067

[a] $R_1 = \sum||F_o| - |F_c||/\sum |F_o|$. [b] $wR_2 = \{\sum[w(F_o^2 - F_c^2)^2]/\sum[w(F_o^2)^2]\}^{1/2}$.

General Procedure for the UV−Visible−NIR Spectroscopic Characterization of Cation Radicals. Cation−radicals and the dication of **D**-br-**D** were prepared by chemical oxidation of neutral donors via electron exchange with the aromatic cation radical **OMN**$^{\bullet+}SbCl_6^-$ (E^o_{red} = 1.34 V vs SCE) generated in situ by the addition of nitrosonium salt $NOSbCl_6$ in anhydrous dichloromethane. All spectra were recorded with a Cary 500 UV−visible−NIR spectrometer. Spectra of the cation radicals of **D**−**D**$^{\bullet+}$ and **D**$(ph)_nH^{\bullet+}$ (n = 1, 2) were obtained by adding 1 equiv of the 1e oxidant **OMN**$^{\bullet+}SbCl_6^-$ to the solution of neutral donor **D**−**D**, and **D**$(ph)_n$H, respectively. Spectra of the cation−radical **D**-br-**D**$^{\bullet+}$ and the dication **D**-br-**D**$^{2+}$ were obtained by spectral titration as follows. A 1-cm quartz cuvette equipped with a Schlenk adaptor was charged under an argon atmosphere with 3 mL of a freshly prepared solution of **OMN**$^{\bullet+}$ $SbCl_6^-$ (generated in situ from $NOSbCl_6$ in anhydrous dichloromethane) and the spectrum recorded. Strong absorption centered at λ_{max} = 673 nm was observed (see Figure 10, the upper spectrum at 673 nm), and the concentration of the oxidant was based on the absorbance at 673 nm[44] ([**OMN**$^{\bullet+}$] = 0.12 mM). A solution of 10 mM donor (**D**$(ph)_2$**D**) in dichloromethane was added to the oxidant solution in 3-μL increments. At the beginning of the titration, the intensity of the 673-nm band decreased and a Gaussian band centered at λ_{max} = 1130 nm was formed with increasing intensity. The absorption decrease at 673 nm and the absorption increase at 1130 nm were proportional to the amount of the added donor until 15 μL of donor (**D**$(Ph)_2$**D**) solution was added (Figure 10). An isosbestic point was observed at 715 nm. At this juncture, the added donor corresponds to $^1/_2$ equiv of the oxidant (**OMN**$^{\bullet+}$)—indicating the 1 equiv of **OMN**$^{\bullet+}$ reacted with $^1/_2$ equiv of neutral donor (**D**$(ph)_2$**D**) to form the dication **D**$(ph)_2$**D**$^{2+}$

$$^1/_2\mathbf{D}(ph)_2\mathbf{D} + \mathbf{OMN}^{\bullet+} \rightarrow {}^1/_2\mathbf{D}(ph)_2\mathbf{D}^{2+} + \mathbf{OMN} \qquad (10)$$

This spectrum was taken as the spectrum of the dication, **D**$(ph)_2$**D**$^{2+}$. As the titration was continued, the intensity of the band centered at 673 nm remained relatively invariant, and the intensity increase of the band centered at 1130 nm diminished. The absorption maximum was red-shifted; the band shape became less Gaussian. Another isosbestic point was observed at 1130 nm, and the absorption in the low-energy region (1700−2200 nm) increased (Figure 10), indicating the comproportionation reaction between the dication (**D**$(Ph)_2$**D**$^{2+}$) and the neutral donor to reversibly generate the cation radical (**D**$(ph)_2$**D**$^{\bullet+}$).

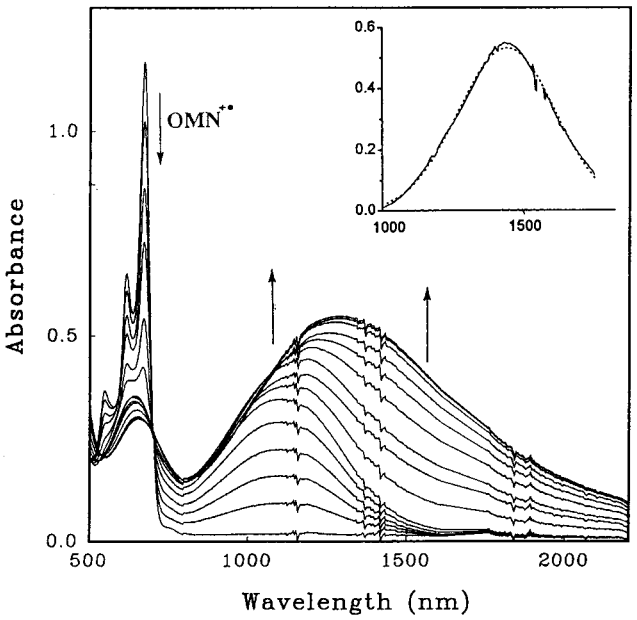

Figure 10. Spectral changes attendant upon the addition of the biphenylene-bridged donor to the paramagnetic (1e) oxidant **OMN**$^{\bullet+}$ showing the initial appearance of the dication **D**$(ph)_2$**D**$^{2+}$ with λ_{max} = 1150 nm followed by the cation−radical **D**$(ph)_2$**D**$^{\bullet+}$ as the result of the comproportionation equilibrium. The inset shows the resolved (Gaussian) intervalence band of **D**$(ph)_2$**D**$^{\bullet+}$obtained by digital subtraction of **D**$(ph)_2$**D**$^{2+}$ (measured initially) from the final spectrum.

$$\mathbf{D}(ph)_2\mathbf{D}^{2+} + \mathbf{D}(ph)_2\mathbf{D} \rightleftarrows 2\mathbf{D}(ph)_2\mathbf{D}^{\bullet+} \qquad (11)$$

After 4 equiv of the donor was added, the spectrum was invariant and taken to be that of the cation radical **D**$(ph)_2$**D**$^{\bullet+}$. At this point, the comproportionation equilibrium was greatly shifted to the right, and the amount of the dication was spectroscopically negligible. The spectral titration of other donors in Chart 1 was carried out by the same procedure.

ESR Spectra of the Mixed-Valence Cation Radicals. The cation radicals for the ESR study were generated from freshly prepared solution of **OMN**$^{\bullet+}SbCl_6^-$ in anhydrous dichloromethane as described above. The spectra were obtained from a Varian E-line Century Series ESR spectrometer from +20 to −100 °C. Static ESR spectra simulations were carried out with PEST WinSim program, version 0.96 (Public

(44) Rosokha, S. V.; Kochi, J. K. *J. Am. Chem. Soc.* **2001**, *123*, 8985.

EPR Software Tools, National Institute of Environmental Health Sciences), by variation of the splitting parameters and line widths to obtain the best correspondence of simulated and calculated spectra. As the starting set of parameters, those of the parent $\mathbf{D}CH_3^{\bullet+}$ were used.[19] The parameters obtained (hyperfine splitting constants and line widths in G, the number of nuclei in parentheses): $\mathbf{D}(ph)H^{\bullet+}$, $a_{OMe} = 3.35$ (6), $a_{CH3} = 4.20$ (3), $a_H = 0.4$ (1), $a_H = 0.6$ (1), line width 1.2. $\mathbf{D}-\mathbf{D}^{\bullet+}$, $a_{OMe} = 1.56$ (12), $a_{CH3} = 2.75$ (6), $a_H = 0.25$ (4), line width 0.4, $\mathbf{D}(ph)\mathbf{D}^{\bullet+}$, $a_{OMe} = 1.45$ (12), $a_{CH3} = 2.60$ (6), $a_H = 0.4$ (2), $a_H = 0.30$ (2), line width 0.60. $\mathbf{D}(ph)_2\mathbf{D}^{\bullet+}$, $a_{OMe} = 3.10$ (6), $a_{CH3} = 4.40$ (3), $a_H = 0.5$ (2), line width 1.2. $\mathbf{D}(CH_2)_3\mathbf{D}^{\bullet+}$, $a_{OMe} = 3.0$ (3), $a_{CH3} = 4.1$ (3), $a_H = 0.4$ (2), $a_{CH2} = 3.8$ (2), $a_{CH2} = 1.5$ (2), $a_{CH2} = 0.3$ (2) (three latter splittings corresponds to bridge hydrogens), line width 0.8.

Dynamic ESR spectra simulations were carried out for $\mathbf{D}(ph)_2\mathbf{D}^{\bullet+}$ and $\mathbf{D}(CH_2)_3\mathbf{D}^{\bullet+}$ with the aid of the ESR-EXN program.[20] In these cases, the parameters obtained in the static ESR simulation for the mononuclear model cation radical were used as the starting point, and the rate constants were varied to obtain the best correspondence between the calculated and experimental spectra. The electron-transfer rate constants obtained from the line-broadening experiments were most reliable in a rather narrow (temporal) range: $3 \times 10^6 < k_{ET} < 10^8\ s^{-1}$. At slower rates, the line broadening was insufficient to be observed, and at faster rates, the line broadening was too severe. When the ET rate constant became very high on the ESR time scale ($>10^9\ s^{-1}$), line narrowing was observed with increasing rate constants, the values of the hyperfine splittings became nearly half, and the number of nuclei doubled as compared with those at the slow-rate limits. Moreover, we were not able to carry out precise dynamic ESR spectra simulations in the limit of fast-exchange rate. We concluded that the charge distribution in $\mathbf{D}(ph)\mathbf{D}^{\bullet+}$ is probably delocalized on the ESR time scale. Furthermore, because the requisite line width [necessary for the appropriate (static) simulation of the ESR spectra of $\mathbf{D}(ph)\mathbf{D}^{\bullet+}$] is larger than those in $\mathbf{D}-\mathbf{D}^{\bullet+}$, the rate constant for electron exchange between the redox centers in the cation radical $\mathbf{D}(ph)\mathbf{D}^{\bullet+}$ is slower (presumably of the order of $10^{10}-10^{11}\ s^{-1}$).

Acknowledgment. We thank Professor S. F. Nelsen for kindly providing the ESR-EXN simulation program, R. Rathore for carrying out some initial studies,[8] and the R.A. Welch Foundation and National Science Foundation for financial support.

Supporting Information Available: The X-band ESR spectrum of the model cation radical $\mathbf{D}(ph)H^{\bullet+}$ together with its computer simulation (Figure 1S), the temperature-dependent ESR spectra of $\mathbf{D}(CH_2)_3\mathbf{D}^{\bullet+}$ at 20 and −80 °C (Figure 2S), and the Arrhenius plot of the intramolecular electron-transfer rate constant (k_{ET}) obtained from the ESR spectra in the temperature range from −100 to 20 °C (Figure 3S), as well as X-ray crystallographic data for the bridge mixed-valence systems **D**-br-$\mathbf{D}^{\bullet+}$ (Tables S1−S35). This material is available free of charge via the Internet at http:// pubs.acs.org. See any current masthead page for ordering information and Web access instructions.

JA011579J